Top Catal (2009) 52:1323–1333
DOI 10.1007/s11244-009-9310-5

ORIGINAL PAPER

Advances in Infrared Spectroscopy of Catalytic Solid–Liquid Interfaces: The Case of Selective Alcohol Oxidation

Davide Ferri · Alfons Baiker

Published online: 9 June 2009

Abstract Progress in the use of ATR-IR spectroscopy to improve the understanding of liquid-phase heterogeneous catalytic reactions is illustrated using the example of the oxidation of benzyl alcohol over Pd/Al_2O_3 and $Bi–Pd/Al_2O_3$. The in situ studies performed in both batch and continuous reactor cells provide rich information on the reaction pathway and important facets of the mechanism, such as the nature of active Pd sites and the effect of the Bi-promoter. The combination of CO site blocking prior to reaction and isotopic labeling suggests that alcohol dehydrogenation occurs uniformly over Pd nanoparticles, but only selected sites may allow desorption of the product benzaldehyde thus providing the required selectivity. Promotion of Pd/Al_2O_3 using bismuth produces infrared spectra free of adsorbed CO. This information demonstrates that Bi is deposited on selected adsorption sites (terraces rather than defects) and simultaneously confirms that open terraces favor product decomposition. Experiments performed in the continuous reactor cell using different catalyst film thickness show that reactions can be studied under kinetic or mass transfer limited conditions depending on catalyst film thickness. This allowed to study the alcohol oxidation under conditions of oxygen diffusion limitation, which are preferably applied in praxis in order to prevent catalyst deactivation by over-oxidation.

D. Ferri (✉)
Laboratory for Solid State Chemistry and Catalysis, Empa, Ueberlandstrasse 129, 8600 Dübendorf, Switzerland
e-mail: davide.ferri@empa.ch

A. Baiker
Institute for Chemical and Bioengineering, ETH Zurich, Hoenggerberg, Wolfgang-Pauli-Strasse 10, 8093 Zurich, Switzerland

Keywords ATR-IR spectroscopy · Alcohol oxidation · Active sites · Pd/Al_2O_3 · Bismuth · CO site blocking · Effect of promoter

1 Introduction

Liquid-phase reactions play a central role in the fine chemical and pharmaceutical industry. Heterogeneous catalysts are used for various reactions such as C–C and C–N bond formations, selective oxidations and hydrogenations. However, solid catalysts working in the liquid phase are still mainly characterized ex situ (under gas phase or even under UHV conditions) and relatively seldom under conditions relevant to liquid-phase catalysis. Although in the past decade some classic techniques have demonstrated their potential to study materials in a liquid environment, still only few examples exist in heterogeneous catalysis. Fluorescence microscopy [1], sum frequency generation [2], X-ray absorption spectroscopy [3], Raman spectroscopy [4], UV-vis spectroscopy [5] and infrared spectroscopy [6, 7] are promising techniques to characterize in an *operando* approach molecular processes at solid–liquid interfaces.

Infrared spectroscopy is a powerful tool to study molecular mechanisms at interfaces. The level of knowledge reached for catalytic solid–gas interfaces is impressive [8–11]. The intrinsic characteristic of recording molecular vibrations of and at surfaces, which renders infrared spectroscopy the tool of choice for studying molecular adsorption at surfaces, can become a serious limitation when a liquid environment is considered. Many organic solvents and water as well strongly absorb infrared radiation in spectral regions of interest for the elucidation of reaction mechanisms. Moreover, the solvent typically

exhibits far stronger signals than species adsorbed at solid surfaces, owing to the relative density of molecules residing within the path of the infrared radiation. Transmission infrared spectroscopy has been used in the past to study catalytic solid–liquid interfaces and some cell designs have been reported [12]. Deposition of a powder thin film of the catalytic material on the window of a classic transmission spectroscopy cell is still efficient, but it requires the use of cell path lengths (few microns) that seriously limit the presence of the powder films itself. Besides, the choice of the solvent is particularly critical. A better optical geometry favoring the analysis of vibrations at solid surfaces immersed in liquids is that offered by the total internal reflection [13]. An infrared transparent material (internal reflection element) serves as the waveguide and according to the optical properties of the system considered (refractive indices of solid and liquid media) allows interaction of the infrared radiation with only a small portion of the liquid in contact with it. The infrared beam penetrates into the liquid medium for a distance that can be inferior to the thinnest spacer available for transmission spectroscopy. It probes a volume of the liquid which is defined by the distance at which the electric field of the radiation decreases to 1/e of its value at the surface of the waveguide. Hence, ATR-IR spectroscopy reveals an analytical tool suited for in situ reaction monitoring of heterogeneously catalyzed reactions (see for example Refs. [14–16]). However, observation of surface processes in this geometry is questionable because of the use of immersion probes [17, 18]. If a powder film of a solid is deposited within the volume probed by the IR radiation thus ideally replacing most of the solvent molecules, molecular processes occurring on the surface of the solid can be selectively probed [19]. Classic experiments of for example CO [20] and pyridine [21, 22] adsorption can be then performed in a similar way to more common parent transmission and diffuse reflectance adsorption studies. The advantage of this geometry is that the particulate film will sensibly enhance the density of molecules at the interface which can be probed by the infrared radiation [23]. This is extremely important for studies of solid catalysts. Information can be gathered simultaneously from adsorbed as well as from dissolved species such as products of catalytic reactions. Therefore, ATR-IR spectroscopy becomes intrinsically suitable for in situ and *operando* studies [24]. A comprehensive review of the use of attenuated total reflection infrared spectroscopy in heterogeneous catalysis can be found in Ref. [7].

Considerable knowledge has been reached in the past about the reaction mechanism of alcohol oxidation [25–27], and these studies are excellently suited to illustrate the development of spectroscopic methods for catalytic solid–liquid interfaces [5, 28–44]. Therefore, we review here the work aiming at understanding the molecular mechanism of the selective aerobic oxidation of benzyl alcohol on Pd/Al_2O_3-based catalysts. The various novel aspects that have been gained demonstrate the potential and limitations of ATR-IR spectroscopy for the investigation of heterogeneous catalysts in contact with liquids under *operando* conditions. It is important to emphasize that the following discussion is related only to processes occurring on the surface of a powder catalyst in contact with a liquid under conditions relevant to the reaction.

2 Experimental

2.1 The Catalysts

Pd/Al_2O_3 (5 wt%) was purchased from Johnson Matthey [35]; 0.75 wt% Bi—5 wt% Pd/Al_2O_3 was prepared by reduction of $Bi(NO_3)_3$ using hydrogen under mild conditions (liquid phase) [32]. Both materials have been extensively characterized with respect to Pd particle size, distribution of Bi and oxidation states of Bi and Pd. Briefly, Bi can be selectively deposited on Pd nanoparticles (average size 3.4 nm [35]) without affecting their size [43]. Given the low Bi-loading, the fraction of Bi not deposited on Pd (ca. 27% [32]) is assumed not to affect the textural properties of Al_2O_3. Therefore, changes in the chemistry of alcohol oxidation observed with the promoted and unpromoted catalysts can be associated to the modification of Pd particles by Bi [43].

2.2 Coating Preparation

Coatings of Pd/Al_2O_3 and $Bi–Pd/Al_2O_3$ were prepared by evaporation of a suspension of the powder catalyst in high purity water (Merck) on the trapezoidal ZnSe internal reflection element (IRE, 45°, 52 × 20 × 2 mm, Crystran Ltd.). Suspensions of 2.5, 5 and 15 mg_{cat}/mL_{water} (Pd/Al_2O_3 only) were prepared. After drying and removal of material exceeding the geometric area estimated after the design of the cell (40 × 16 mm), the coated IRE was weighed and directly mounted in the homemade stainless steel reactor cell used for the ATR-IR measurements. After mounting, a gap of about 300 μm was formed between the cell wall and the surface of the IRE, through which the reaction solution was passed [35]. The temperature of the cell was regulated using a thermostat. A new particulate film was prepared before each experiment.

Particulate coatings of Pd/Al_2O_3 identical to those used for ATR-IR measurements were prepared on ZnSe fragments and imaged using scanning electron microscopy (SEM), which allowed an estimation of the coating thickness.

2.3 Spectroscopy

ATR-IR measurements were performed using an IFS 66 spectrometer (Bruker Optics) equipped with a liquid nitrogen-cooled MCT detector and a commercial mirror unit (Specac). After placing the cell on the mirror unit and alignment, the sample compartment was allowed to purge for at least 2 h to remove water vapour and CO_2. Measurements were carried out at 50 °C and spectra were obtained after co-addition of 200 scans (scanner velocity of 10 kHz) at a resolution of 4 cm^{-1}. Liquids were pumped through the cell using a peristaltic pump at a flow rate of 0.5 mL/min. Typically, after system stabilization under a flow of Ar-saturated solvent (cyclohexane, Aldrich, >99%) provided by a glass bubble tank, the flowing solution was changed to H_2 and H_2-saturated solvent was allowed to contact the catalyst coating provided by a second glass bubble tank. After about 20 min, the Ar-saturated solution of benzyl alcohol (Aldrich, >99%) was admitted from a third glass bubble tank to the cell to follow the dehydrogenation process. The gas was then changed to synthetic air in the same tank to follow the oxidation process. Finally, Ar-saturated solvent was used to wash the particulate coating. The dehydrogenation and oxidative processes were followed during ca. 30 min and 60 min, respectively.

Experiments aiming at elucidating the difference between Pd/Al_2O_3 and $Bi–Pd/Al_2O_3$ were carried out only with the 5 mg_{cat}/mL_{water} coating. CO-blocking experiments were performed as described above for the benzyl alcohol solution saturated with Ar with the exception that Pd/Al_2O_3 was pre-equilibrated with CO-saturated solvent after reduction and prior to admission of the alcohol solution. Identical CO-blocking experiments were performed with ^{13}C-labeled benzyl alcohol (Aldrich, 99% ^{13}C) [39].

The effluent of the ATR-IR cell was monitored online using transmission infrared spectroscopy [40, 43]. A commercial liquid cell (Specac, CaF_2 windows, teflon spacer, $l = 1$ mm) adapted in house for flow-through measurements was mounted on a separate Tensor 27 spectrometer (Bruker Optics) equipped with a standard DTGS detector. Typically, infrared spectra were measured at 30 s intervals by accumulating 28 scans at a resolution of 4 cm^{-1}. A first spectrum was collected when the ATR-IR cell was still contacted with the H_2-saturated solvent, which served as reference for all other transmission spectra. Reduction under these conditions can be easily followed [43]. The spectrometers were independently triggered to measure and the time required for the liquid to cover the distance between the exit of the ATR-IR cell and the inlet of the transmission cell was 4 min at 0.5 mL/min flow rate.

GC analysis of the effluent of the cell was also performed for comparison using a Thermo Quest Trace 2000 equipped with an HP-FFAP capillary column and FID detector. Samples were taken at regular intervals during an experiment by collecting the solution exiting the reactor cell. During the change from dehydrogenative to oxidative conditions, the sampling frequency was increased in order to better follow changes in catalytic activity.

3 Results and Discussion

3.1 Reaction Mechanism

In fine chemistry many liquid-phase reactions catalyzed by a solid are typically performed in stirred batch reactors in which the heterogeneous catalyst is suspended in the reaction mixture consisting of solvent, reactants, and products (slurry reactor). Selective alcohol oxidation is such a reaction. According to the principle of *operando* spectroscopy it is crucial to describe the state of the catalyst while it is functioning under conditions relevant to the process in consideration. Implicitly, this means that also the type of reactor needs to be simulated in such an approach [45]. Figure 1 shows preliminary spectra of the 5 wt% Pd/Al_2O_3 catalyst in contact with a solution of benzyl alcohol in which air is bubbled and which is contained in a stainless steel batch reactor cell fitted with the coated ZnSe internal reflection element [46]. Beside the main signal of the product benzaldehyde (1713 cm^{-1}, υ(C=O)), which could be directly used to determine alcohol conversion, major signals populate the spectra that can be assigned to products of side reactions. The densely populated spectra of Fig. 1 can provide first hands-on information on the reaction mechanism and the distribution of products under conditions typical of a lab-scale catalytic run.

In order to gather more information on the reaction mechanism of a catalytic reaction a flow-through cell as the one described in Ref. [35] is more convenient because conditions can be changed repeatedly without for example the limitation of accumulation of the product in the reactor cell. This has been done for the selective alcohol oxidation under conditions similar to those described above for the batch reactor cell. However, the experiments on alcohol oxidation have been typically split in two phases in which the solvent is first saturated with Ar and then with air (instead of pure oxygen) [36]. Since there is agreement that the reaction obeys the dehydrogenation mechanism [47], the phase with inert gas should provide information on the dehydrogenation reaction, whereas the phase in which air is used should provide information on the role of oxygen in the reaction.

We have focused our attention mainly on the oxidation of benzyl alcohol and this reaction was chosen as a test

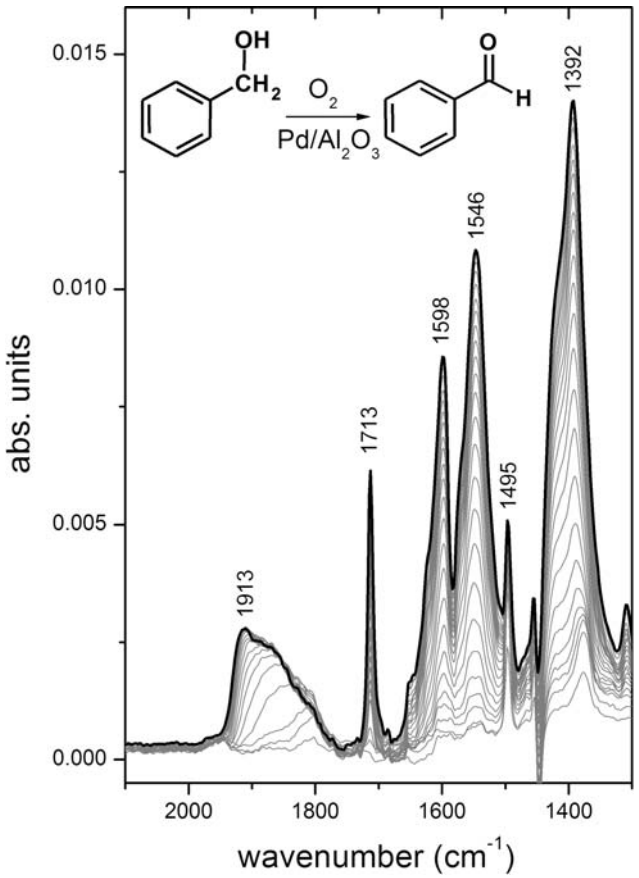

Fig. 1 ATR-IR spectra during benzyl alcohol oxidation with air following reduction with H_2-saturated solvent. The spectra were acquired at 50 °C while stirring the alcoholic solution in cyclohexane (15 mL) over a thin film of 5 wt% Pd/Al_2O_3 (10 mg) deposited on a ZnSe internal reflection element placed at the bottom of a homemade stainless steel batch reactor cell [46]. Spectra were collected every 2.5 min over 2 h reaction time. The negative feature at ca. 1450 cm^{-1} is given by incomplete solvent compensation

reaction because of the rich information contained in the ATR-IR spectra [35, 36]. Beside benzyl alcohol, other alcohols have been used for the ATR-IR experiments and the results have been used to demonstrate the effect of alcohol structure on its reactivity [35]. The use of alcohols whose oxidation cannot afford the corresponding carboxylic acid (such as 1-phenylethanol and 1-octanol) demonstrates the formation of water at the solid–liquid interface as a result of the reaction. Water is not detectable using benzyl alcohol.

Figure 2 shows the scanning electron micrographs of three powder thin films of the 5 wt% Pd/Al_2O_3 deposited on the ZnSe internal reflection element, which were prepared with different amounts of material. From an optical point of view the films appeared homogeneous and no areas exposing ZnSe were observed within the area delimited by the particulate film. Figure 2 also shows the online FTIR response to the signal of benzaldehyde (1713 cm^{-1}) produced in the ATR-IR cell and measured as a function of time in the transmission IR cell. Therefore, these results provide information on the reactivity of the three powder films in the reactor ATR cell. Despite minor differences in the production of benzaldehyde in the Ar-phase, the three materials appear to exhibit the same catalytic performance. The profiles show two maxima in benzaldehyde production, which reflect the chemical changes occurring on the catalyst surface. After a first maximum under dehydrogenation conditions that is always within the first 20 min of contact of benzyl alcohol with the catalyst, the signal of benzaldehyde (i.e. yield) reaches a minimum indicating that the catalyst has been deactivated. In the presence of oxygen, the activity is boosted by a factor 3–4 (up to 15% yield by GC). The maximum of activity developing in air shows an increasing half-width and shifts to longer times with increasing film thickness. After the maximum the activity drops approximately to the activity level achieved after the maximum of the dehydrogenation phase, which can be best observed for the thinnest film. Similar information for both phases is gained from the GC analysis of samples taken every 5 min (not shown). It should be reminded here that the data of the online FTIR (and GC) provide information on the solution exiting the ATR-IR cell and therefore represent an integral view of what occurred in the reactor cell. Moreover, the online FTIR spectra exhibit only signals of benzyl alcohol and benzaldehyde throughout the experiment. Only the GC data are able to demonstrate that toluene is produced in the Ar-phase and that irrespective of film thickness selectivity to benzaldehyde increases up to ca. 50% at the minimum conversion before the switch to air. Toluene cannot be detected by infrared spectroscopy because its spectrum strongly overlaps with the other signals.

Figure 3 shows the species evolving on the catalyst surface in the case of the three films in the same experiments as shown in Fig. 2 in the Ar- and air-phases. The spectra resemble those observed in Fig. 1 and present the features typical of the oxidation of benzyl alcohol on Pd [35, 36]. The detail assignment of all signals and the corresponding species has been provided in Ref. [36]. Benzaldehyde (1713 cm^{-1}), benzyl alcohol (1495–1450 cm^{-1}), benzoate species ($C_6H_5COO^-$, below 1600 cm^{-1}) and adsorbed CO (above 1750 cm^{-1}) are observed. Benzoate species mask the presence of water. Comparison of the data of Figs. 2 and 3 demonstrates the necessity to follow the molecular processes on the catalyst surface because analysis of the liquid phase only cannot provide information on important side reactions affording CO and benzoic acid (as benzoate) in the specific case of benzyl alcohol oxidation [36]. Observation of CO during reaction allowed gathering information on active sites (see following section) [39].

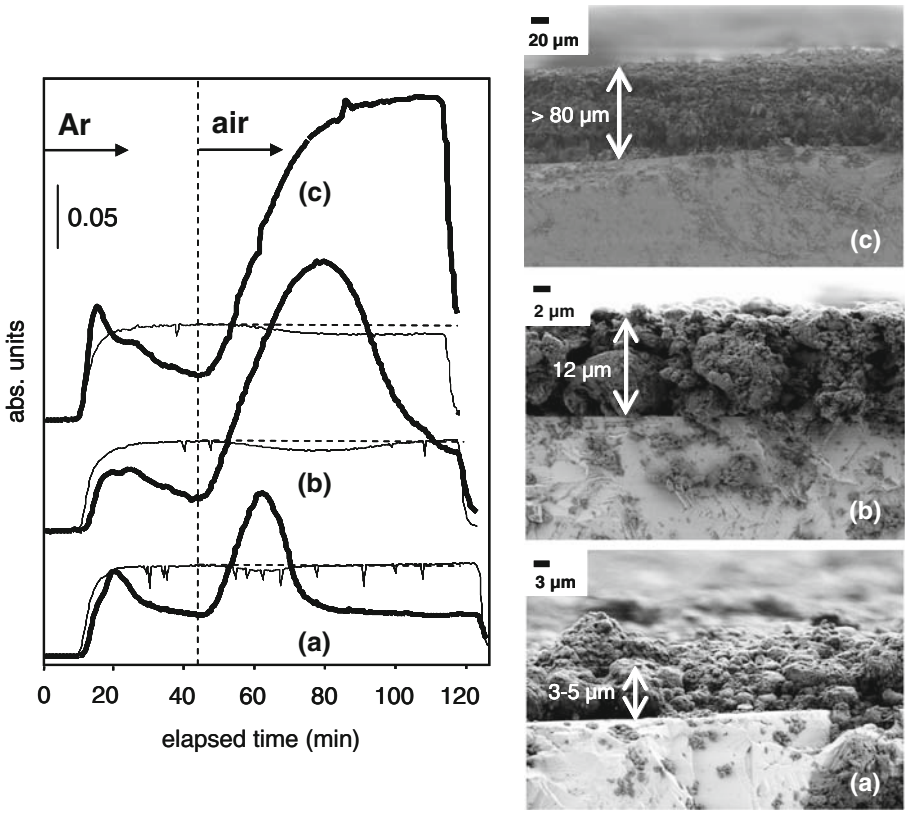

Fig. 2 Cross sectional SEM images of the three Pd/Al_2O_3 particulate films and online transmission FTIR profiles of the signals at 1713 cm^{-1} (benzaldehyde, thick line) and 1395 cm^{-1} (benzyl alcohol, thin line) during benzyl alcohol oxidation using combined ATR-IR-FTIR. **a**, **b** and **c** correspond to films obtained from suspensions of 2.5, 5 and 15 mg_{cat}/mL_{water} of 5 wt% Pd/Al_2O_3 deposited on ZnSe. The corresponding ATR-IR spectra recorded during these experiments are shown in Fig. 3. Conditions: 50 °C, cyclohexane solvent (Ar and air), $C_{alcohol} = 0.2$ M, 0.5 mL/min

As mentioned, the development of all these signals on the catalyst surface is closely related to the dehydrogenation mechanism of alcohols on Pd [26, 27, 48], which we aimed at characterizing using ATR-IR spectroscopy. The spectra shown in Fig. 3 provide information on at least three different reactions occurring during benzyl alcohol oxidation, which are partly summarized in Scheme 1 for Pd/Al_2O_3: alcohol dehydrogenation already occurring in the absence of oxygen and affording adsorbed hydrogen (reaction a); product decarbonylation to CO and benzene (which can be easily hydrogenated to cyclohexane, the solvent of the experiment)[reaction b]; and benzaldehyde oxidation to benzoic acid [36] (not shown in Scheme 1). The latter remains adsorbed most likely on Al_2O_3 as benzoate and is not observed in online FTIR and GC. The presence of toluene in the gas chromatograms reveals as mentioned that hydrogenolysis is also occurring. This reaction, together with the observation of adsorbed CO suggests that reduced Pd is available for reaction. Indeed, experiments performed with and without reduction prior to admittance of benzyl alcohol proved that alcohol oxidation requires Pd^0, an issue that is still debated [40, 49, 50]. In situ reduction of the noble metal nanoparticles was demonstrated using ATR-IR spectroscopy and X-ray absorption spectroscopy [43]. Bürgi attributed the changes observed on the same catalyst in combined ATR-IR and UV-vis spectroscopic measurements to particle dissolution and re-precipitation according to the Ostwald ripening mechanism [5].

Scheme 1 also displays consumption of adsorbed hydrogen (from alcohol dehydrogenation, reaction c) thus producing water, and re-oxidation of Pd by molecular oxygen (reaction d), which causes catalyst deactivation.

The data shown in Figs. 1 and 3 cannot be used to detect the reaction intermediate of the dehydrogenation process, which has been postulated using UHV methods [51]. This has been shown to be possible at the solid–liquid interface as well using modulation excitation spectroscopy combined with ATR-IR in the case of the oxidation of isopropanol [31].

Interestingly, Fig. 3 shows a trend in the growth of the different signals which is depending on film thickness. The observation that the amount of CO produced from benzaldehyde decomposition and the amount of dissolved benzaldehyde increase, whereas the amount of adsorbed benzoate species decreases with increasing film thickness can be understood in terms of an oxygen gradient through the particulate film. The volume of catalyst probed by the infrared radiation within the particulate film is nearly the same in the three experiments, while the film thickness changes. Moreover, in the three experiments oxygen reaches the point of measurement nearly at the same time. This is indicated by the steep increase in benzaldehyde signal in Fig. 2 that is identical for the three films. This

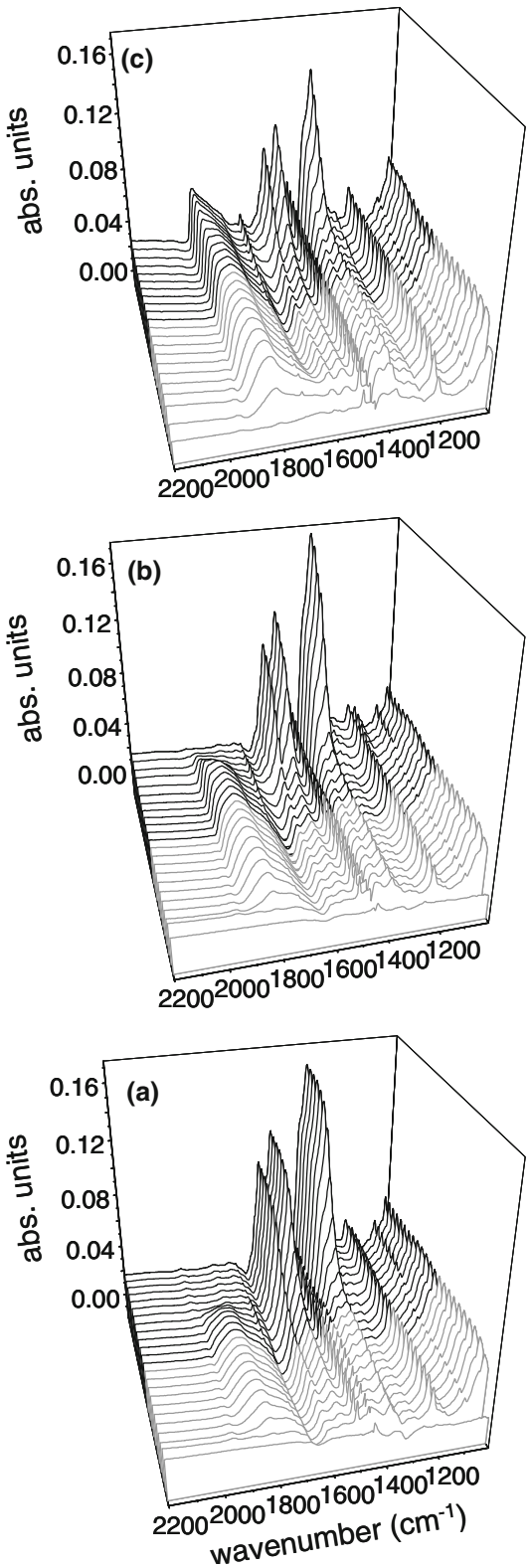

◀**Fig. 3** ATR-IR spectra collected during benzyl alcohol oxidation on 5 wt% Pd/Al_2O_3 films of varying thickness: **a** 2.5, **b** 5 and **c** 15 mg_{cat}/mL_{water}. Gray and black spectra indicate the dehydrogenation (Ar) and the oxidative (air) phases, respectively. The three experiments were collected simultaneously to the online FTIR data shown in Fig. 2. Conditions: 50 °C, cyclohexane solvent (Ar and air), $C_{alcohol}$ = 0.2 M, 0.5 mL/min

phenomenon is obviously much less important in the case of the thinnest film (Fig. 3a), where the film thickness is closer to the penetration depth of the infrared radiation (ca. 0.9 μm at 1700 cm^{-1}). In this latter case, given the lower amount of catalyst, oxygen quickly saturates the surface and causes deactivation in short time. However, in the thickest film (Fig. 3c), oxygen is already consumed by the top layers of the film that are not probed by ATR-IR. Oxygen is in fact responsible for cleaning the Pd nanoparticles for example from co-adsorbed hydrogen (from alcohol dehydrogenation) and CO [28] (reaction c in Scheme 1). This behaviour is seen in Figs. 2 and 3. When activity increases due to the presence of oxygen, CO is consumed. However, excess oxygen is causing catalyst deactivation, a phenomenon often described as over-oxidation [52–54]. With increasing amount of catalyst, the amount of benzaldehyde increases in the presence of air but oxygen is also more consumed to clean the noble metal surface and to allow keeping it active for dehydrogenation. Therefore, the thickest catalyst film is more resistant towards deactivation and the spectra are most likely representing a situation in which alcohol dehydrogenation, product decarbonylation, product oxidation and water formation due to oxygen are balanced. This experiment is therefore more similar to a real batch reactor run in which oxygen has to be carefully dosed in order to prevent deactivation [54]. The spectroscopic experiments shown here demonstrate in terms of surface species why alcohol oxidation is preferentially performed under oxygen mass transfer limitation [47].

Water would be a direct evidence for deactivation of the catalyst due to over-oxidation, because it is the product of the reaction between oxygen and adsorbed hydrogen originating from alcohol dehydrogenation (Scheme 1, reaction c). However, as mentioned above, water is not visible in the spectra collected using benzyl alcohol as the reactant (see for example Fig. 1). A better candidate for providing this information is 1-phenylethanol [35]. Figure 4a shows the difference spectra obtained by subtracting the first spectrum measured after switching from dehydrogenation conditions to air from all recorded spectra in the oxidative phase. The sharp signal at 1695 cm^{-1} corresponds to dissolved acetophenone, the product of 1-phenylethanol oxidation. The spectra also clearly display a broader signal at 1625 cm^{-1} which can be readily attributed to water formed in situ during reaction. The spectra are free of adsorbed acid species, since acetophenone cannot be further oxidized to carboxylic acid. The two signals have a comparable behaviour on time (Fig. 4b), but the signal of the oxidation product grows in first followed by that of water and after passing

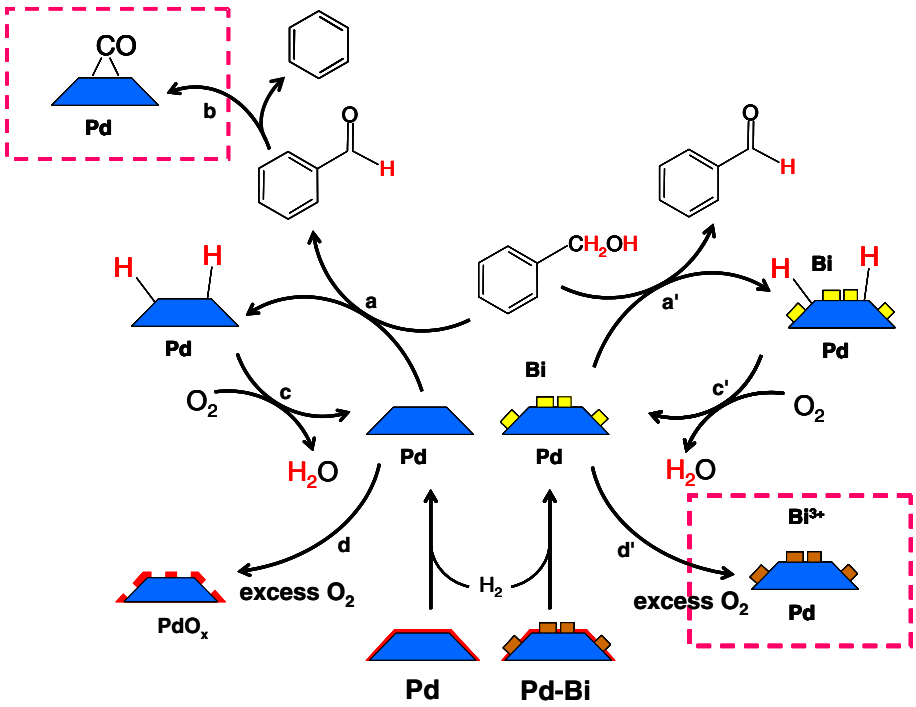

Scheme 1 Details of the reaction mechanism of benzyl alcohol oxidation evinced using ATR-IR spectroscopy adapted from Refs. [36] and [40]. Only reactions in which Pd is involved are shown. The difference between Pd and Pd–Bi systems is exaggerated, meaning that certain processes are not completely suppressed by the presence of Bi but are hindered. The dashed boxes indicate the major effects of Bi as found using ATR-IR spectroscopy. The first step, reduction of both catalysts is performed in situ in the reactor cell in order to provide reduced Pd for reaction. Oxidation of benzaldehyde to benzoic acid is not shown for simplicity and it could be catalyzed by the support (see Ref. [36]). Benzene was not observed in the ATR-IR experiments, since the spectrum of liquid-phase benzene strongly overlaps with other signals evolving during reaction; additionally, it is most likely hydrogenated to cyclohexane (the solvent used in the experiments shown in all figures) on Pd. Adsorbed hydrogen (2H) originates from benzyl alcohol dehydrogenation (reactions a and a')

through a maximum rapidly attenuates. Similar behaviour is observed for the signal of water but with a certain delay. The GC data provide a measure of the activity detected in the reactor cell for 1-phenylethanol oxidation and well match the ATR-IR data. The experiment shows that when oxidation to acetophenone starts to be inhibited, water is present on the catalyst and maybe taken as an evidence for over-oxidation.

It is interesting to note how adsorbed CO coexists with dissolved oxygen especially in the case of the thickest Pd/Al_2O_3 layer (Fig. 3c) and in the batch reactor cell (Fig. 1), where bridge sites on defects and (100) planes become populated with increasing reaction time. Moreover, the dehydrogenation reaction occurs even in case of site blocking by CO indicating that the deactivation observed under dehydrogenation conditions results in fact from the inhibiting effect of co-adsorption of hydrogen atoms from the twofold dehydrogenation of the alcohol and only partially by CO adsorption. The observation of CO during reaction has been used to elucidate which metal sites may be involved in alcohol dehydrogenation and in benzaldehyde decarbonylation and this is described in the following paragraph.

3.2 Active Sites

In the experiments carried out in the flow-through reactor cell as in Fig. 3, CO originating from decarbonylation of benzaldehyde exhibits a signal at 1853 cm^{-1} with a number of shoulders during the liquid-phase oxidation of benzyl alcohol on Pd/Al_2O_3 under dehydrogenation conditions (Ar-saturated solvent). According to the literature assignment of adsorbed CO on Pd nanoparticles [55], the low frequency of the signal indicates that during dehydrogenation CO occupies predominantly hollow sites on (111) planes. This assignment agrees quite well with the preferential adsorption of CO on (111) faces of well-defined Pd nanoparticles contaminated by carbon deposits upon exposure to methanol [56] and with the selective perturbation of the vibration of CO adsorbed on step sites by adsorbed Xe [57].

Given the co-existence of CO and benzyl alcohol dehydrogenation (Figs. 1 and 3), CO site-blocking has been used to characterize the sites responsible for alcohol dehydrogenation and product decarbonylation. This has been done by saturating the Pd nanoparticles with CO prior to admission of the solution of benzyl alcohol and Ar

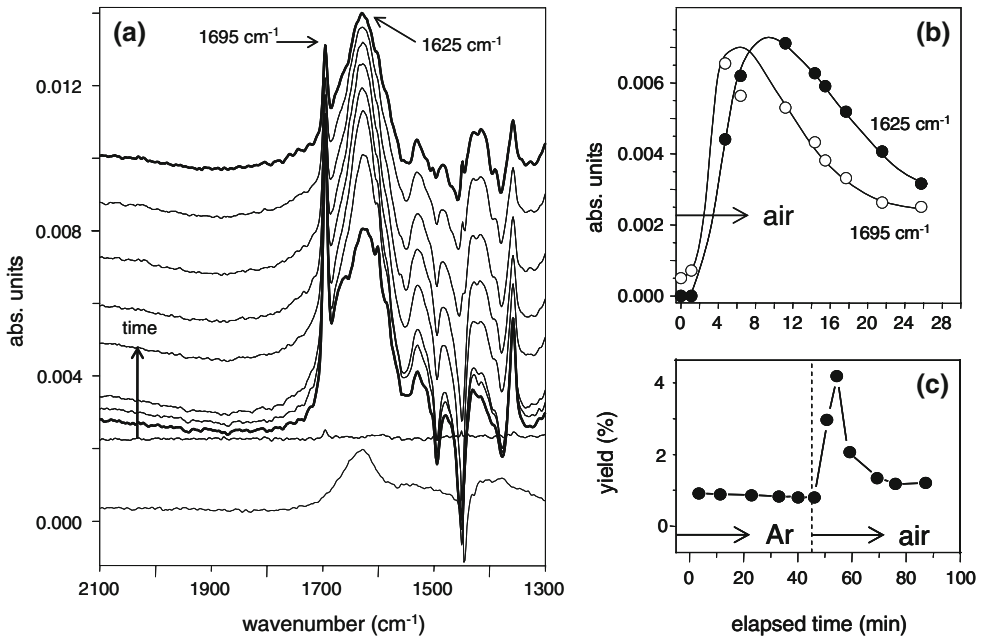

Fig. 4 **a** ATR-IR spectra during 1-phenylethanol oxidation on 5 wt% Pd/Al_2O_3 under oxidative conditions (air). Reference spectrum is in this case the first spectrum measured under air. Negative signals arise from consumption of 1-phenylethanol at the solid–liquid interface. The bottom spectrum was obtained by admitting a water/cyclohexane mixture over Pd/Al_2O_3 after reduction. **b** Evolution of the intensity of the signals of acetophenone (1695 cm^{-1}) and water (1625 cm^{-1}) with time on stream under oxidative conditions. **c** Corresponding activity data as measured by GC under dehydrogenative and oxidative conditions. Conditions: 50 °C, cyclohexane solvent (Ar and air), $C_{alcohol} = 0.2$ M, 0.5 mL/min

(dehydrogenation phase) into the reactor cell. The ATR-IR spectra show that the CO signals are perturbed likely due to disruption of CO dipole-dipole interactions induced by benzyl alcohol: the signal at 2074 cm^{-1} is attenuated and that at 1968 cm^{-1} shifts to ca. 1950 cm^{-1} and is enhanced (Fig. 5) [39]. CO adsorbed in the on-top geometry on corner sites (2074 cm^{-1}) does not appear strictly related to the catalytic activity, since these sites are liberated almost immediately. On the contrary, the on-top geometry on edge sites (ca. 2050 cm^{-1}) follows a similar trend to the signal at 1968 cm^{-1}. Catalytic activity monitored by the appearance of the signal at 1713 cm^{-1} of dissolved benzaldehyde is observed only when the signal originally at 1968 cm^{-1} is suddenly consumed [39] (Fig. 5, spectra at 123 min on stream). At this point a broad CO signal extends between 1950 and 1700 cm^{-1}, which resembles the CO feature observed in the Ar-phase during benzyl alcohol oxidation on the pre-reduced Pd/Al_2O_3 without CO blocking (Fig. 3). This experiment demonstrates that benzaldehyde formation clearly occurs under dehydrogenation conditions when CO is completely removed from bridge sites.

An identical experiment using benzyl alcohol labeled with ^{13}C at the methylene group reveals that what remains on Pd after reaction ignition does not originate from benzaldehyde decarbonylation, but is residual CO from the pre-equilibration of Pd/Al_2O_3 with CO. Moreover, this CO is strongly adsorbed predominantly on (111) planes. The strategy behind the use of labeled alcohol lies in the fact that dehydrogenation should afford benzaldehyde labeled at the carbonyl carbon atom and the decarbonylation of this product should provide ^{13}CO. Owing to the isotope effect the signals of carbonyl-containing species evolving during oxidative dehydrogenation of labeled benzyl alcohol are red-shifted compared to those shown in Figs. 1 and 3. After pre-equilibration of Pd/Al_2O_3 with CO and admission of the solution of ^{13}C-benzyl alcohol (Fig. 5b), no ^{13}CO is detected when ^{13}C-labeled benzaldehyde appears and the shape of the remaining CO signal is identical to that obtained with unlabeled benzyl alcohol (Fig. 5a) and to that obtained without CO blocking (Fig. 3).

The selective site blocking achieved using CO provides evidence that benzyl alcohol displaces CO from bridge sites (most likely on corner and edges) and reacts to benzaldehyde only when these sites are liberated. Additionally, it provides important information on the product decarbonylation, which could contribute to catalyst deactivation under dehydrogenation conditions. Benzaldehyde desorbs intact from the sites from which CO is displaced by benzyl alcohol and does not decompose on those sites where CO is more strongly bound (envelope between 1950 and 1700 cm^{-1}). Since the signal at 1853 cm^{-1} observed during benzyl alcohol dehydrogenation on the untreated Pd catalyst (Fig. 3) resembles the feature observed during the same reaction on the catalyst pre-equilibrated with CO

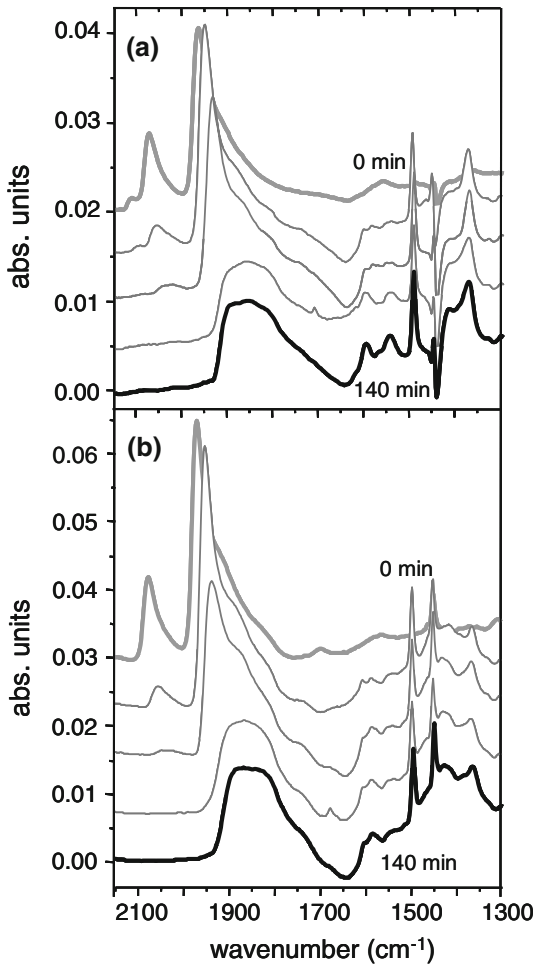

Fig. 5 ATR-IR spectra collected during benzyl alcohol dehydrogenation following CO blocking of 5 wt% Pd/Al_2O_3: **a** benzyl alcohol and **b** ^{13}C-labeled benzyl alcohol. Spectra are stacked (top spectrum: CO pre-equilibration, bottom spectrum: end of experiment) to better appreciate the appearance of benzaldehyde simultaneous to the disappearance of the main CO signal at 1968 cm^{-1}. Conditions: 50 °C, cyclohexane solvent (Ar), $C_{alcohol} = 0.2$ M, 0.5 mL/min, pre-adsorbed CO. Spectra were collected approximately at 0, 20, 120, 123 and 140 min on stream in both cases

(Fig. 5a), we have proposed that product decarbonylation occurs preferentially on hollow sites on (111) planes [39]. These findings are in line with the interpretation given for the reactivity of other supported Pd-nanoparticles on which alcohol oxidation was claimed to be structure sensitive, the coordinatively unsaturated Pd atoms acting as the key active species [58]. However, we interpreted our data differently. Benzyl alcohol dehydrogenation is rather structure insensitive, thus occurring indiscriminately on all Pd sites. But product decarbonylation is favored on (111) planes, whereas the product desorption occurs from defects and (100) planes. Therefore, product decarbonylation is structure sensitive, as it was already observed in UHV studies [59], which attributed the apparent structure sensitivity of alcohol reactions on Pd to the different stability of the product on different surfaces. It should be noted that the sites discussed above may also be simultaneously involved in other side reactions observed in the complex mechanism of benzyl alcohol oxidation on Pd/Al_2O_3.

The determination of the nature of the sites affording selectively alcohol dehydrogenation leads to a possible strategy to increase the activity of Pd/Al_2O_3 for alcohol oxidation. Assuming that defect sites such as particle corners and edges are effectively active for this reaction, two routes can be envisaged to increase the overall catalyst selectivity: (i) the design of catalysts with higher dispersion (smaller particles) or with lower metal loading, and (ii) the selective blocking of the sites leading to product decomposition. Assuming that Pd nanoparticles exhibit a cuboctahedron shape the number of edge-atoms should increase and the number of atoms on flat surfaces should decrease with decreasing particle size [60]. Moreover, the number of atoms in planes should decrease if a second metal is selectively deposited as in the case of Bi-promotion. The latter approach was investigated as described in the next section.

3.3 Effect of Promoter

The results obtained by CO site-blocking were further investigated and a reasonable independent proof was found for our assignment of specific metal sites for alcohol dehydrogenation and aldehyde decarbonylation by using Bi as catalyst promoter. The nature of promotion by heavy metals is still debated likely due to the complex phenomena involved in such process [61]. Promotion can dramatically improve the performance of the noble metal-based catalyst. Analysis of Bi-promoted 5 wt% Pd/Al_2O_3 under identical conditions to those shown above including Ar- and air-phases resolved a significant aspect of the complex puzzle of the nature of the promotion for alcohol oxidation catalysts [43]. Bimetallic Pd–Bi catalysts can be prepared by mild liquid-phase reduction such that they are consisting of Bi adatoms or agglomerates deposited selectively on the noble metal particles [32, 39, 62] rather than true bimetallic alloys [63]. Comparison of the ATR-IR spectra recorded under dehydrogenation (Ar) conditions on Pd/Al_2O_3 and $Pd–Bi/Al_2O_3$ indicated that the influence of Bi on the reaction network is in fact remarkable. $Pd–Bi/Al_2O_3$ exhibited an almost negligible amount of CO and less intense benzoate features already under dehydrogenation conditions as shown in Fig. 6. Therefore, Bi clearly inhibits side reactions involving the product like decarbonylation and oxidation to benzoic acid, thus improving 'selectivity'. It should be noted that this 'selectivity' does not correspond to the one measured by conventional gas-chromatography, as CO and benzoate cannot be detected online for quantitative determination of conversion and

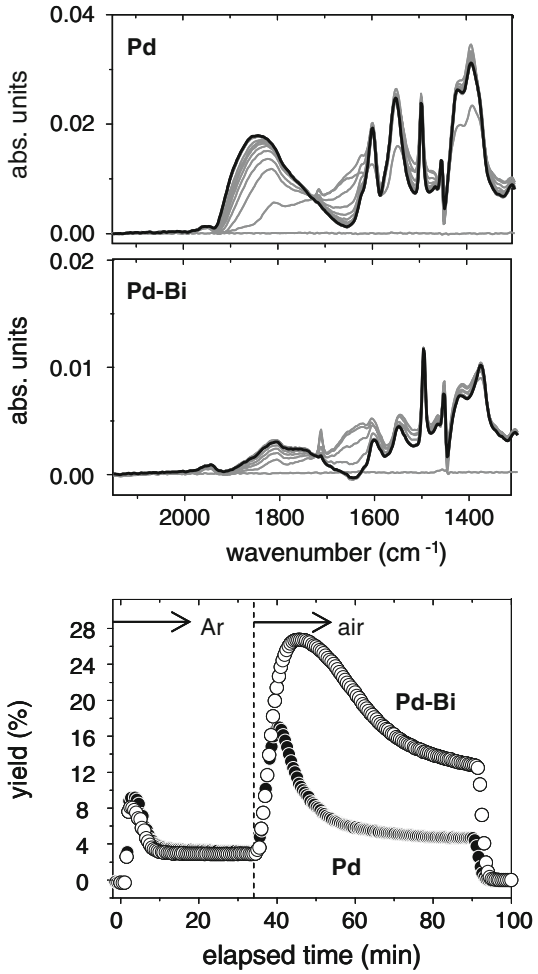

Fig. 6 ATR-IR spectra collected under dehydrogenation conditions during benzyl alcohol oxidation on 5 wt% Pd/Al_2O_3 (Pd) and 0.75 wt% Bi–5 wt% Pd/Al_2O_3 (Pd–Bi), and benzaldehyde yield as derived from online FTIR profiles of the signal at 1713 cm^{-1} obtained during the two ATR-IR experiments. Conditions: 50 °C, cyclohexane solvent (Ar), $C_{alcohol} = 0.2$ M, 0.5 mL/min

selectivity because they remain adsorbed on the catalyst surface (Pd and Al_2O_3). The ATR-IR spectra and the online FTIR spectra revealed that the intensity of the signal at 1713 cm^{-1} is comparable on both materials under dehydrogenation conditions, suggesting that Pd–Bi/Al_2O_3 is more active/selective: it produces as much benzaldehyde as Pd/Al_2O_3 but does not produce CO and benzoic acid. A clear effect of the promoter is to change the product distribution.

Under oxidizing conditions (spectra not shown), the benzoate species were again formed less abundantly on the promoted catalyst. Interestingly, the yield of benzaldehyde (profile of the signal at 1713 cm^{-1}) is larger on Pd–Bi/Al_2O_3 (Fig. 6) and after reaching a maximum decreases although a broader window of activity is observed compared to Pd/Al_2O_3. The data in Fig. 6 reveal that Bi also leads to better control of the oxygen supply to the active Pd surface favoring activity in the presence of oxygen, and both selectivity and efficiency in the absence and in the presence of oxygen. The data indicate that, as already proposed earlier [64], one facet of Bi promotion in alcohol oxidation is the use of Bi as oxygen scavenger [65] (reaction d', Scheme 1). Complementary XAS data to the ATR-IR measurements provided clear evidence that Bi is in fact able to re-oxidize before Pd [43], therefore prolonging the time the noble metal remains in the reduced state and thus active. This behaviour appears to be strongly steered by the nature of the alcohol, as benzyl alcohol seems to possess a much stronger reducing capability than 1-phenylethanol [32].

The ATR-IR data collected on benzyl alcohol oxidation and the resulting information on the reaction mechanism are summarized in Scheme 1, where the difference between Pd/Al_2O_3 and Pd–Bi/Al_2O_3 based catalysts is also depicted.

On Pd/Al_2O_3, several reactions have been identified using ATR-IR spectroscopy and some aspects of the role of oxygen have been clarified [28, 35]: oxygen keeps the metal surface free from poisons such as co-adsorbed CO and hydrogen. Together with the experiments of CO-blocking and isotope exchange, the behaviour of the Pd–Bi/Al_2O_3 found using ATR-IR spectroscopy provided strong support for the assignment made for active metal sites for the reaction [39]. The almost complete absence of adsorbed CO in the presence of Bi under dehydrogenation conditions suggests that the promoter inhibits benzaldehyde decarbonylation (reaction b, Scheme 1). Remembering that Bi is selectively deposited on Pd because of the mild preparation conditions, this observation strongly supports the assignment of the activity of Pd(111) planes towards product decarbonylation. Bi is likely selectively deposited on (111) planes, therefore suppressing product decarbonylation. In Scheme 1 Bi is explicitly depicted as if it was deposited on particle faces and not on edges. Beside other important effects of Bi deposition on Pd/Al_2O_3 which may strongly influence activity and selectivity, site blocking resulting in selectivity enhancement appears to be an important effect of Bi but is certainly only one facet of this challenging question [25, 33, 64].

4 Conclusions

The data presented above and collected in Refs. [35, 36, 39, 43, 46] demonstrate that ATR-IR spectroscopy has the potential to become the tool of choice to study molecular processes at the surface of heterogeneous catalysts in contact with a liquid. Although the technique is intrinsically apt for *operando* studies due to the fact that information is obtained from both dissolved and adsorbed

species, combination with an online method (FTIR, UV-vis) or more generally with an analytical tool (GC, HPLC) is even more powerful to uncover structure-activity relationships.

Besides providing rich information on the overall reaction mechanism with observation of several by-products, combination with selective site blocking by co-adsorbed CO and isotope labeling facilitated the discrimination of the different sites active in the liquid-phase oxidative dehydrogenation of benzyl alcohol on Pd/Al_2O_3. The study on the nature of the promoter on alcohol oxidation may open an interesting route to compare bimetallic and monometallic catalysts that are often used in liquid-phase heterogeneous catalytic reactions. Therefore, ATR-IR spectroscopy is also likely to become a powerful tool for investigating the nature and the effect of alloy formation in the environment in which the catalyst operates.

Acknowledgments The authors kindly acknowledge the Foundation Claude and Giuliana for the financial support. We thank Dr. C. Keresszegi and Dr. C. Mondelli for their precious contribution to this work, Dr. F. Krumeich for taking the SEM and HR-TEM images, R. Mäder and M. Küpfer from the mechanical workshop of ETH for manufacturing the infrared cells, Prof. J.D. Grunwaldt and Dr. T. Mallat for valuable discussions.

References

1. Roeffaers MBJ, Sels BF, Uji-i H, De Schryver FC, Jacobs PA, De Vos DE, Hofkens J (2006) Nature 439:572
2. Waldrup SB, Williams CT (2007) Catal Commun 8:1373
3. Grunwaldt JD, Baiker A (2005) Phys Chem Chem Phys 7:3526
4. Cheong CUA, Stair PC (2007) J Phys Chem C 111:11314
5. Bürgi T (2005) J Catal 229:55
6. Ma Z, Zaera F (2004) Catal Lett 96:5
7. Bürgi T, Baiker A (2006) Adv Catal 50:227
8. Armaroli T, Becue T, Gautier S (2004) Oil Gas Sci Technol 59:215
9. Topsoe NY (2006) Catal Today 113:58
10. Lamberti C, Groppo E, Spoto G, Bordiga S, Zecchina A (2007) Adv Catal 51:1
11. Rupprechter G (2007) Adv Catal 51:133
12. Rochester CH (1980) Adv Colloids Interface Sci 12:43
13. Harrick NJ (1967) Internal reflection spectroscopy. Interscience, New York
14. Rekoske JE, Barteau MA (1995) Ind Eng Chem Res 34:2931
15. Hamminga GM, Mul G, Moulijn JA (2004) Chem Eng Sci 59:5479
16. Pintar A, Malacea R, Pinel C, Fogassy G, Besson M (2004) Appl Catal A Gen 264:1
17. Mul G, Hamminga GM, Moulijn JA (2004) Vibr Spectrosc 34:109
18. Tromp SA, Mul G, Zhang-Steenwinkel Y, Kreutzer MT, Moulijn JA (2007) Catal Today 126:184
19. Bürgi T, Wirz R, Baiker A (2003) J Phys Chem B 107:6774
20. Ebbesen SD, Mojet BL, Lefferts L (2007) J Catal 246:66
21. Billingham J, Breen C, Yarwood J (1996) Clay Mineral 31:513
22. Ferri D, Frauchiger S, Bürgi T, Baiker A (2003) J Catal 219:425
23. Wang Z, Larsson ML, Grahn M, Holmgren A, Hedlund J (2004) Chem Commun 2888
24. Weckhuysen BM (2004) In situ spectroscopy of catalysts. American Scientific Publisher, Stevenson Ranch, California
25. Gallezot P (1997) Catal Today 37:405
26. Besson M, Gallezot P (2000) Catal Today 57:127
27. Mallat T, Baiker A (2004) Chem Rev 104:3037
28. Keresszegi C, Bürgi T, Mallat T, Baiker A (2002) J Catal 211:244
29. Grunwaldt JD, Keresszegi C, Mallat T, Baiker A (2003) J Catal 213:291
30. Keresszegi C, Grunwaldt JD, Mallat T, Baiker A (2003) Chem Commun 2304
31. Bürgi T, Bieri M (2004) J Phys Chem B 108:13364
32. Keresszegi C, Grunwaldt J-D, Mallat T, Baiker A (2004) J Catal 222:268
33. Keresszegi C, Mallat T, Grunwaldt JD, Baiker A (2004) J Catal 225:138
34. Burgener M, Wirz R, Mallat T, Baiker A (2004) J Catal 228:152
35. Keresszegi C, Ferri D, Mallat T, Baiker A (2005) J Catal 234:64
36. Keresszegi C, Ferri D, Mallat T, Baiker A (2005) J Phys Chem B 109:958
37. Opre Z, Grunwaldt JD, Mallat T, Baiker A (2005) J Mol Catal A Chem 242:224
38. Burgener M, Tyszewski T, Ferri D, Mallat T, Baiker A (2006) Appl Catal A Gen 299:66
39. Ferri D, Mondelli C, Krumeich F, Baiker A (2006) J Phys Chem B 110:22982
40. Grunwaldt JD, Caravati M, Baiker A (2006) J Phys Chem B 110:25586
41. Haider P, Baiker A (2007) J Catal 248:175
42. Haider P, Grunwaldt JD, Baiker A (2007) J Catal 250:313
43. Mondelli C, Ferri D, Grunwaldt JD, Krumeich F, Mangold S, Psaro R, Baiker A (2007) J Catal 252:77
44. Mondelli C, Ferri D, Baiker A (2008) J Catal 258:170
45. Banares M (2006) Catal Today 113:48
46. Ferri D, Mäder R, Grunwaldt JD, Mondelli C, Panella B, Vargas A, Baiker A (in preparation)
47. Di Cosimo R, Whitsides GM (1989) J Phys Chem 93:768
48. Heyns K, Paulsen H (1962) Adv Carbohydr Chem 17:169
49. Markusse AP, Kuster BFM, Koningsberger DC, Marin GB (1998) Catal Lett 55:141
50. Lee AF, Hackett SFJ, Hargreaves JSJ, Wilson K (2006) Green Chem 8:549
51. Davis JL, Barteau MA (1990) Surf Sci 235:235
52. van Dam HE, Kieboom APG, van Bekkum H (1987) Appl Catal 33:361
53. Dijkgraaf PJM, Rijk MJM, Meuldijk J, van der Wiele K (1988) J Catal 112:329
54. Kluytmans JHJ, Markusse AP, Kuster BFM, Marin GB, Schouten JC (2000) Catal Today 57:143
55. Lear T, Marshall R, Lopez-Sanchez JA, Jackson SD, Klapötke TM, Bäumer M, Rupprechter G, Freund HJ, Lennon D (2005) J Chem Phys 123:174706
56. Schauermann S, Hoffmann J, Johanek V, Hartmann J, Libuda J, Freund HJ (2002) Angew Chem Int Ed 41:2532
57. Xu J, Henriksen PN, Yates JT (1994) Langmuir 10:3663
58. Mori K, Hara T, Mizugaki T, Ebitani K, Kaneda K (2004) J Am Chem Soc 126:10657
59. Shekhar R, Barteau MA (1995) Catal Lett 31:221
60. van Hardeveld R, Hartog F (1969) Surf Sci 15:189
61. Wenkin M, Ruiz P, Delmon B, Devillers M (2002) J Mol Catal A Chem 180:141
62. Rodriguez P, Solla-Gullon J, Vidal-Iglesias FJ, Herrero E, Aldaz A, Feliu JM (2005) Anal Chem 77:5317
63. Karski S, Witonska I (2003) J Mol Catal A 191:87
64. Mallat T, Baiker A (1994) Catal Today 19:247
65. Besson M, Gallezot P, Lahmer F, Flèche G, Fuertes P (1995) J Catal 152:116